Ultrafast Science
A SCIENCE PARTNER JOURNAL

Review Article
Broadband THz Sources from Gases to Liquids

Yiwen E [iD],[1] **Liangliang Zhang,**[2] **Anton Tcypkin,**[3] **Sergey Kozlov** [iD],[3] **Cunlin Zhang,**[2] **and X.-C. Zhang** [iD][1]

[1]*The Institute of Optics, University of Rochester, NY 14627, USA*
[2]*Department of Physics, Capital Normal University, Beijing 100048, China*
[3]*ITMO University, St. Petersburg 199034, Russia*

Correspondence should be addressed to X.-C. Zhang; xi-cheng.zhang@rochester.edu

Matters are generally classified within four states: solid, liquid, gas, and plasma. Three of the four states of matter (solid, gas, and plasma) have been used for THz wave generation with short laser pulse excitation for decades, including the recent vigorous development of THz photonics in gases (air plasma). However, the demonstration of THz generation from liquids was conspicuously absent. It is well known that water, the most common liquid, is a strong absorber in the far infrared range. Therefore, liquid water has historically been sworn off as a source for THz radiation. Recently, broadband THz wave generation from a flowing liquid target has been experimentally demonstrated through laser-induced microplasma. The liquid target as the THz source presents unique properties. Specifically, liquids have the comparable material density to that of solids, meaning that laser pulses over a certain area will interact with three orders more molecules than an equivalent cross-section of gases. In contrast with solid targets, the fluidity of liquid allows every laser pulse to interact with a fresh area on the target, meaning that material damage or degradation is not an issue with the high-repetition rate intense laser pulses. These make liquids very promising candidates for the investigation of high-energy-density plasma, as well as the possibility of being the next generation of THz sources.

1. Introduction

With tremendous advancements in laser technology, light-induced ionization in matter including gases [1–6], clusters [7–9], liquids [10–16], and solids [17–20] has attracted considerable interest in generating coherent, intense, and broadband terahertz (THz) waves via nonlinear processes. When a laser intensity is above the ionization threshold, abundant electrons and ions are created [21–23]. These charged particles can generate transient currents radiating electromagnetic (EM) waves, which cover the spectrum from microwaves to X-rays [2, 24, 25]. The laser-induced air plasma has become one of the most popular THz sources, generating THz waves with a field strength over the MV/cm level under two-color (fundamental and its second harmonic beams) optical excitation [26, 27]. This opens up a new avenue of extreme THz science [28]. Moreover, detecting fluorescence and acoustic waves from a plasma is crucial in characterizing the process

of laser-matter interaction. With an external THz field, the fluorescence and acoustic wave of a plasma can be enhanced via the collision process of accelerated particles. THz radiation-enhanced emission of fluorescence (THz-REEF) [29–31] and THz field-enhanced acoustics (TEA) [32, 33] have been demonstrated for detecting broadband and coherent THz waves remotely.

THz wave generation from air plasma was firstly observed by Hamster et al. [1] in 1993 by focusing optical beams into a small volume of ambient air. It is awe-inspiring due to its simplicity. A THz source is achieved by using only one single lens. The photoexcited electrons in air plasma experience a ponderomotive force due to the density-gradient distribution, moving towards the areas with lower electron density. Since electrons cannot move faster than the laser beam, the plasma density is kept identically in the laser propagation direction resulting in that electrons are accelerated in the backward direction to create a dipole

along the direction of laser propagation [1, 2, 34]. The THz wave emitted from the single-color air plasma shows a conical energy distribution [35].

In 2000, it was reported by Cook and Hochstrasser [3] that the generation efficiency of THz waves from laser-induced gas-plasma is significantly enhanced under two-color excitation. This technology is a milestone in the THz community due to its capability of generating an intense THz pulse with a peak field of over MV/cm as well as an ultrabroad bandwidth. For the two-color air plasma, THz wave can be coherently controlled by individually tuning the polarization and phase of each optical beam [5, 36, 37]. The generation process and the capability of coherent control can be interpreted by a four-wave mixing model [3, 5], a transient current model [38–40], and a full quantum mechanical model numerically solving the time-dependent Schrödinger equation [41]. In the reciprocal process, ionized gas matter with a high third-order susceptibility is correspondingly used to detect ultra-broadband THz pulses through the process of THz field-induced second harmonic generation [42, 43]. The THz air-biased coherent detection (THz-ABCD) is capable of detecting the entire THz spectrum without the limitation of the phonon absorption existing in crystal detectors [44].

To boost THz generation efficiency, some efforts have been done in ionized noble gases [45] and atomic clusters [8, 9]. However, further studies reveal electron density saturation and laser intensity clamping effects [46, 47]. Meanwhile, plasma produced in solid material shows advantages in generating intense THz waves. In 2008, Sagisaka et al. firstly reported THz wave generation from moving electrons on a solid target surface [48]. From then on, the record of THz pulse energy has been constantly created in solid targets [17]. Recently, it has been observed by Liao et al. that THz pulse energy exceeding millijoule (mJ) is generated from picosecond laser-irradiated metal foils [18]. For a solid target, it is difficult to realize a continuous replenishing for each pulse. Usually, the target is replaced for each pulse. The single-shot measurement is needed for detecting the signal. Instead, liquid targets can be circulated easily by adding a pump system. The recent demonstration of THz wave generation from liquid targets has attracted considerable attention due to its superiorities.

The demonstration of using liquids as a THz source was firstly reported in different geometries by two groups in 2017. Jin et al. observed THz wave generation from a thin, free-standing water film [10]. Dey et al. reported THz wave generation from ionized liquids by focusing intense laser into a cuvette [11]. With successive studies [12–15, 49–51], THz wave generation from liquids shows different properties comparing to that from other targets. In this paper, we review recent studies of THz wave generation from flowing liquid targets as well as the ultrafast dynamics of liquids under intense THz excitation. A comparison of THz wave generation from air plasma and liquid plasma is also provided. Different liquids as THz sources are discussed in detail. Terahertz liquid photonics shows a potential to develop new-type THz sources and also offers a new perspective to investigate the process of laser-liquid interaction.
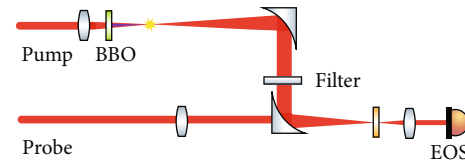

FIGURE 1: A typical THz two-color air plasma system. The laser beam is split into the pump beam and probe beam. The air plasma is produced by focusing the pump beam. One BBO crystal is inserted to create the second harmonic pulse. The THz signal is detected via electro-optic sampling (EOS).

2. THz Wave Generation from Air

The THz generation process in air plasma is intimately tied with gas ionization; it requires that the intensity of the optical pulse is greater than $10^{12}\,\mathrm{W/cm^2}$. This can be achieved through geometric focusing of intense laser pulses with lenses or curved mirrors. When the pulse intensity exceeds the ionization threshold, a plasma channel with a mm to cm length is formed in air. This plasma channel stabilizes the beam at very small diameters (30 to $100\,\mu\mathrm{m}$) and maintains high intensities over ranges much longer than the Rayleigh length of a traditional, geometrically focused beam. The THz wave is emitted by the transient current formed in the air plasma.

Figure 1 shows the schematic of a typical two-color air plasma system. The femtosecond laser beam is split into the pump beam and the probe beam. The pump beam is focused into air to create an air plasma, generating THz waves. After passing through THz filters, the THz signal is coherently measured by the probe beam via either electro-optical sampling (EOS) or ABCD. The excitation by using one fundamental beam is known as single-color excitation. Two-color excitation is realized by inserting a frequency doubling crystal, usually beta barium borate (BBO), into the focused pump beam to generate the second harmonic pulse. Then, both fundamental and its second harmonic beams are focused into air to create a plasma. Comparing to the THz signal under single-color excitation, the THz field from two-color air plasma is 3 orders higher with a much broader bandwidth.

3. THz Wave Generation from Water

Compared with gaseous material, liquids are easier to be ionized due to the relatively low critical potential [52–54]. As the most common liquid on Earth, water has strong cohesion, adhesion, and surface tension, which are beneficial in forming a free-standing liquid target with a smooth surface. It is also colorless, transparent, chemically stable, nontoxic, and inodorous. These properties make water one of the ideal objects for the research community. Besides, water is an excellent solvent for a wide variety of substances. To study the THz wave generation from water, the same setup as shown in Figure 1 is employed and a thin liquid target is inserted at the focal point. Instead of an air plasma, ionization in liquid is created.

3.1. Flowing Liquid Targets. Solid and liquid materials have a similar molecular density, which is about 3 orders higher
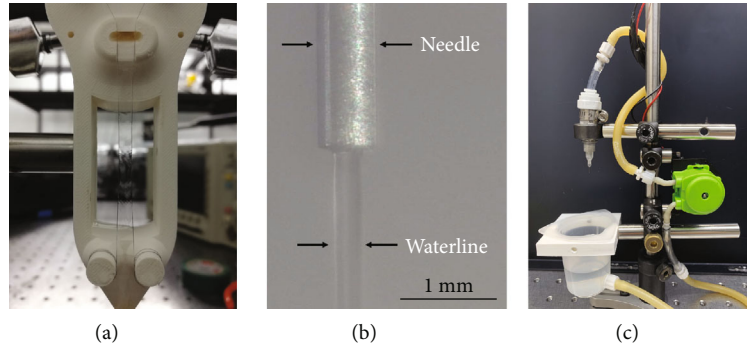
FIGURE 2: Liquid targets and the liquid system. (a) A gravity-driven water film. The thickness is 210 μm. (b) A pump-driven water line with a diameter of 260 μm, which is guided by a syringe needle. (c) A home-built liquid system, which needs only 50 ml water for several hours running. A syringe is used as a jet for producing a liquid line.

than that of gas at the standard ambient temperature and pressure. However, it is hard to reproduce the results because of the target surface degradation under intense laser excia-tion. Instead, the fluidity of a liquid target is able to provide a fresh area for each pulse. Benefiting from this, the influence between optical excitation pulses can be eliminated. Using liquid targets as sources has been studied for decades in the generation of extreme ultraviolet radiation and X-ray for the requirement of the laser-induced high-density plasma [55–57]. For THz wave, however, most liquids show very strong absorption. Such as the most common liquid—water, the absorption coefficient at 1 THz is about 220 cm^{-1} [58, 59]. In order to reduce absorption of the THz signal in water, the target with a thickness less than 500 μm is required for THz wave generation [10].

The flowing target can be driven either by the gravity or by a pump. Figure 2(a) shows a gravity-driven water film, in which the film is guided by two parallel metal wires. The transparency in the visible range of the film indicates a thin thickness as well as the smoothness of the film sur-face. The surface tension of liquid water is relatively high, which is able to support a film with thickness in several micrometers. The thickness of the film can be tunable by varying the flow rate or the gap between the parallel wires. A higher flow rate produces thicker films. A liquid jet is another way of making a flowing target. A circulating sys-tem can be easily made by pumping liquids from a collect-ing reservoir to nozzles. The liquid jet can be shaped by the nozzle shape. Figure 2(b) shows a pump-driven water line. In this case, a syringe needle with an inner diameter of 260 μm works as a nozzle. Figure 2(c) is a home-built liquid line system, which consists of a peristaltic pump, a jet (syringe needle), a liquid reservoir, and some pipes. This system is compact and easy to be built, which is able to produce the liquid lines with diameters from 90 μm to 510 μm by using different syringe needles. Moreover, a test with hours of operation shows that it only needs 50 ml liq-uid material in the circulating system. Also, the liquid line from this system is very stable and has an excellent liquid-air interface. It should be noted that the smoothness of the liquid target surface is important to get a better focus of the laser beam without too much scattering.

To calibrate the thickness of a water film precisely, we can use an optical autocorrelation system by inserting the film into one of the two laser beams [60]. Figure 3(a) shows the measured results. The black line is the original signal from the autocorrelation system without a water film. After insert-ing the water film, the signal peak in time domain delays to a certain position because of the different optical path caused by the water film. The peak position moves linearly with the increase of the film thickness. Figure 3(b) shows the linear dependence of the thickness on the flow rate. In our case, the thickness of the wire-guided water film can be varied contin-uously from 50 μm to 350 μm. The accuracy of the controlled film thickness is within 20 μm.

3.2. Single-Color Optical Excitation. THz wave generation from liquids was firstly demonstrated under single-color excitation. Because the thickness of a liquid target is much thinner than 1 mm, to confine most pulse energy in the tar-get, the length of ionization region should be shorter than the thickness. Therefore, creating a microplasma in the liquid is needed by focusing a laser beam via a high-numerical aper-ture (NA) objective [34].

Figure 4(a) is a photo of a microplasma induced by a 0.85 NA air immersion microscope objective in ambient air, where the laser pulse energy is 65 μJ. The fluorescence spot at the focal point is shown in Figure 4(b). These lon-gitudinal and transverse sizes of this microplasma are smaller than 30 μm, which are measured by an iCCD cam-era. Figure 4(c) is the measured THz field as a function of the THz emission angle. The direction of the maximum THz emission is nearly perpendicular with respect to the optical axis. We attribute this sideways THz radiation to the steep ponderomotive potential at the focal plane, which accelerates the free electrons created by photoioni-zation. The comparison of microplasmas with the elon-gated plasmas is summarized in Table 1. The concept of a microplasma is employed for exploring THz wave gener-ation from thin liquid targets, meaning a lens with a short focal length is used in the setup.

Because of the high molecular density, scattering and nonlinear effects in water are much stronger than those in air. By focusing a laser beam with the same pulse energy
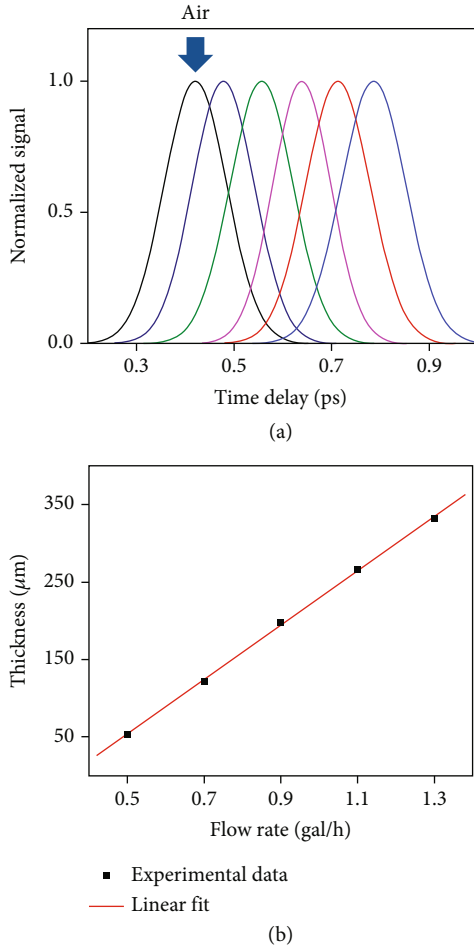
(a)

(b)

FIGURE 3: Calibration of the water film thickness. (a) The original (air) signal from the autocorrelation system is plotted in the black line. With the water film inserted in one of the two laser beams of the autocorrelation system, the signal peak will move linearly with the increase of film thickness. (b) The linear dependence of the film thickness on the flow rate. The thickness of the water film can be continuously varied from 50 μm to 350 μm.

and pulse duration, the fluorescence is much brighter in water. Figure 5(a) is a photo of a flowing water line, which is ionized by a tightly focused laser beam. Here, a 2-inch focal lens is used. By using a traditional THz time-domain spectroscopy system, a THz waveform is measured in the forward direction (laser propagation direction). Figure 5(b) shows a typical THz pulse emitted from water. This signal is detected via EOS, which has a dynamic range over 1100 and a signal-noise ratio (SNR) better than 300 when the pump pulse energy is 0.4 mJ. Here, the dynamic range is calculated by the ratio of the signal peak level and the noise level of the system (the minimum signal of the system), which indicates the detection range of a system. And the SNR is calculated by the ratio of the maximum signal and the fluctuation of the maximum signal itself, which describes the stability of a system. The relatively low SNR mainly results from the vibration of the liquid target surface. The inset shows the corresponding spectrum. The central wavelength is close to 0.5 THz, which is limited to the strong water absorption at higher frequency.

In contrast to gas target without interfaces, the liquid and solid targets bear the target/air interfaces in the generation process. Because most solid metal targets are not transparent to the optical laser beam and THz wave, the detection is generally conducted in a reflection geometry. For a free-standing transparent liquid target, the transmitted geometry is in favor. The system can be optimized by air plasma first, and then, it can be switched for studying of the liquid generation process by inserting a liquid target at the focus without changing other optical elements. In this case, the optical beam is refracted at the air/liquid interface first. Because water is easier to be ionized than air, the ionization sometimes starts at the surface when the optical intensity exceeds the ionization threshold of water but lower than that of air. The refraction angle of the optical beam is a key parameter for maximizing the THz signal. Figure 6(a) shows normalized THz energy with respect to the incidence angle (α). The positive and negative signs of α indicate that the film is rotated in a clockwise or counterclockwise direction, respectively. The squares show the THz energy obtained from the integral of the THz waveforms. The error is the standard deviation of multiple measurements. The solid line is a simulation result based on a dipole approximation model, in which the electrons in the ionized area experience the ponderomotive force and create a dipole along the direction of laser propagation. Both, the experimental and simulated results show that the THz field is maximized when the incidence angle is about 65°, which results from the transmittance of the p-polarized excitation laser at the air/water interface and the dipole orientation direction caused by the refraction of the surface. Figure 6(b) plots THz waveforms generated from the water film when the incidence angle is ±65°. The THz field has the same peak value but opposite polarity. The insets show the experimental geometry and the flipped direction in the projection of the dipole (red arrow) for two cases. The opposite direction of the dipole projection results in the flipped waveforms accordingly.

Another influence of the target/air interface is the total internal reflection for the emitted THz wave, which greatly decreases the transmission of THz wave at the flat surface. In other words, a liquid line or droplet target could offer stronger THz signals than the flat film. Zhang et al. demonstrated intense THz radiation from a water line [15]. Instead of rotating the water film to get an optimized incidence angle, the THz signal from a liquid line is optimized by scanning the position of the liquid line across the laser focus. During the movement, the effective thickness in the waterline varies continuously, as well as the optical incidence angle. A similar incidence angle dependence but a much stronger signal is obtained by using a water line than a water film with the comparable thickness.

One remarkable property of THz wave generation from liquid is the preference of the longer optical pulse duration [10, 50]. Figure 7 plots the dependence of THz energy on the optical pulse duration. For air plasma, the maximum THz signal is always obtained when the laser pulse is close to the Fourier transform-limited pulse. Higher peak power always leads to a stronger ionization in the air case. However, THz wave generation from liquids surprisingly prefers a

(a)   (b)   (c)
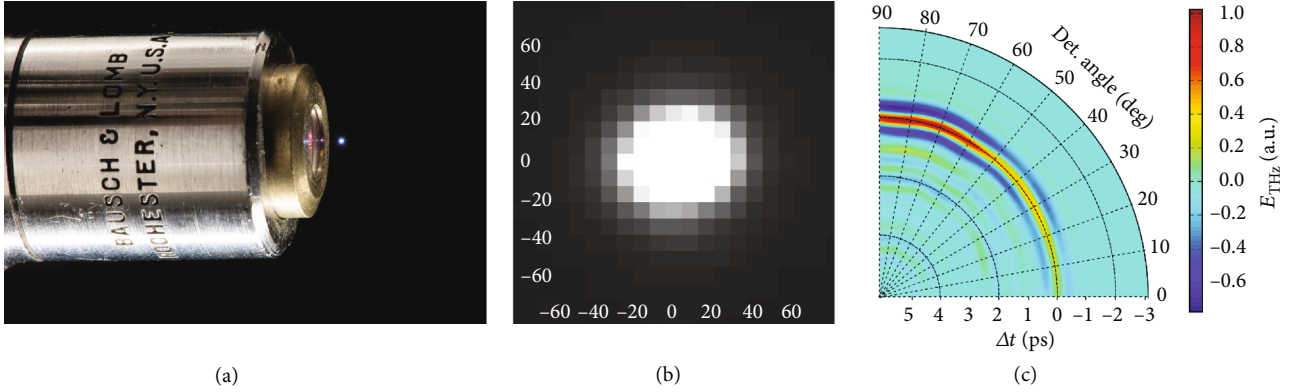
FIGURE 4: Microplasma and the signal distribution [34]. (a) A photo of the microplasma fluorescence obtained by focusing the laser beam with a high NA microscope objective. (b) A magnified image of the microplasma (unit is μm). However, the plasma spot's contribution to the THz wave is about one micrometer or less. (c) Measured THz field as a function of the THz emission angle. The optimal angle is 80 degrees from the laser propagation direction.

TABLE 1: Comparison between microplasma and elongated plasma under the same pump energy.

Microplasma	Filament (elongated plasma)
Length: <500 μm	Length: few mm up to meters
Width: <10 μm	Width: ~100 μm
Tight focusing of the laser (NA > 0.1)	Loose focusing of the laser (NA $\ll$ 0.1)
Higher peak laser intensity (>5 × 10^{14} W/cm^2)	Lower peak laser intensity (~ 1 × 10^{14} W/cm^2)
Higher peak electron densities (~ 10^{18} – 10^{19} cm^{-3})	Lower peak electron densities (~ 10^{15} – 10^{16} cm^{-3})
Position does not change with laser energy	Position changes with laser energy
Lower laser energy threshold (<1 μJ)	Higher laser energy threshold (~ 50 μJ)

longer pulse. As shown in Figure 7, the THz signal increases with an increased pulse duration by adding a frequency chirp in the pulse. At a certain pulse duration, the THz signal reaches its maximum. By comparing the THz spectra generated by negatively and positively chirped pulses, we did not find apparent difference in both the bandwidth and amplitude, which suggests that the chirp of the laser pulse does not play an important role here. Instead, pulse duration is the key parameter. This phenomenon can be explained by the different ionization processes in liquid and air. A high molecular density of liquid causes a more frequent collision. The mean-free time of ionized electrons is about 1 fs in liquid [61], leading to hundreds of cycles of collisions that happened within the ionization process when the pulse duration is subpicosecond. Therefore, the electron density in water is mainly determined by the cascade ionization process. However, multiphoton and tunneling ionization are more important in the case of gas. For more information on the theoretical analysis about single-color excitation, please check [15, 50, 62, 63].

3.3. THz Emission in the Sideways Direction. Similar to THz wave generation from a microplasma in air, a thin liquid target can also emit THz wave in the sideways directions. Figure 8(a) schematically illustrates the system for the sideways measurement, in which the THz radiation propagating perpendicular to z direction is measured by a sideways detector. For a fair comparison, the forward detector measures the signal in the z direction by using the same EOS crystal to assure the same detection efficiency. The pump beam is focused by a 2-inch focal length lens onto a water line. Figure 8(b) shows the comparison of THz waveforms generated from water and air. Here, a 210 μm thick water line is used as a THz source. The pump pulse energy is 0.4 mJ for all cases. All the signals are optimized for getting the maximum signal by tuning the pulse duration. In this case, the optimal pulse duration is about 534 fs. And the shortest pulse duration (~140 fs) is used for the air plasma generation. The results show that the THz signal generated from water is much stronger than that from ambient air. And the THz signal generated from air plasma is mainly in the forward direction. There is no detectable THz signal from air in the sideways direction in this case. To get the sideways signal from air plasma, a lens with a higher NA is needed. However, the signal from liquid water in the sideways direction is about twice as much as that of its forward signal. The corresponding spectra are shown in Figure 8(c). Both signals from water in the sideways and forward directions shows a narrower bandwidth than that from air plasma. The strong sideways THz signal might result from the strong scattering from the liquid or the shorter longitudinal dimension of the "micro water plasma" caused by the much higher molecular density
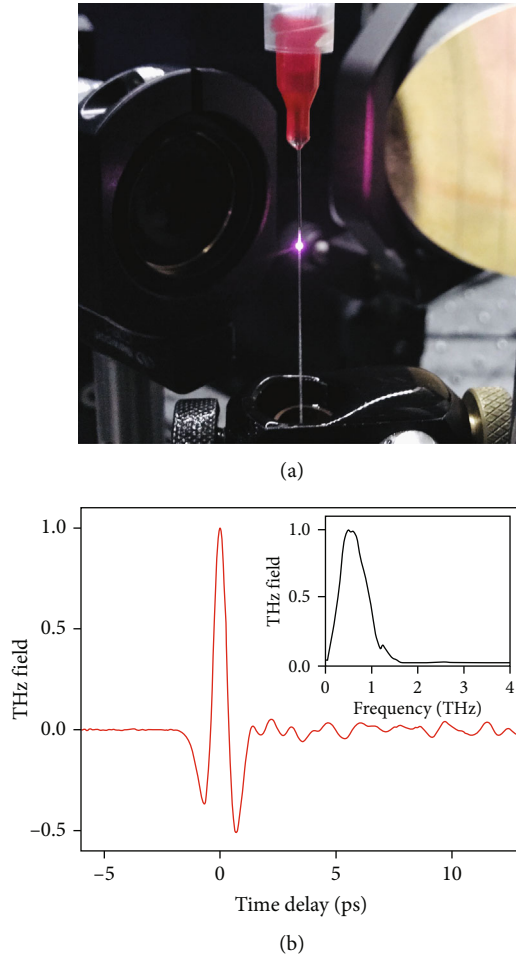
(a)

(b)

FIGURE 5: THz generation from liquid water under single-color ionization. (a) A photo of a fluorescence from a laser-induced microplasma of a water line. (b) A typical THz waveform generated from a water line and its corresponding spectrum (inset).
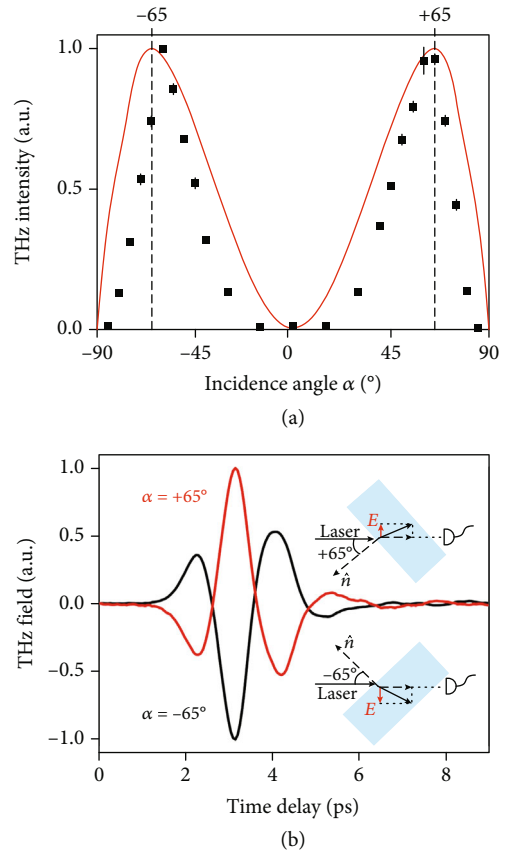

(a)

(b)

FIGURE 6: The dependence of the THz signal on the incidence angle α [10, 12]. (a) THz intensity with different incidence angles is studied by rotating the water film. The THz signal is maximized when α is 65°. The squares are the experimental results, and the red line is a simulated result from a dipole model. (b) Two THz waveforms obtained with opposite incident angles. The insets explain the observation with a contribution of the flipped dipole projection (E) of opposite incidence angles.

in liquid. This observation also confirms that the THz generation from liquid water has a much higher efficiency than that from air.

3.4. Two-Color Optical Excitation. By mixing the fundamental beam and its second harmonic beam, THz wave generation efficiency from gas-plasma is greatly improved, which is usually known as two-color excitation. A similar enhancement is expected to improve the THz signal from liquid. However, instead of several orders of enhancement, the THz field generated from liquid water under two-color excitation is about 10 times stronger than that from the one-color excitation scheme [13]. This may be caused by the short mean free-path length of the electrons in water, which results in a decrease of transient photocurrent [39, 61]. Alternatively, ionized electrons in liquid are quasi free and less sensitive to the asymmetric field.

Similar to the gas case, by precisely tuning the phase between the fundamental and its second harmonic beams, the THz field can be coherently modulated [13]. Figure 9(a)
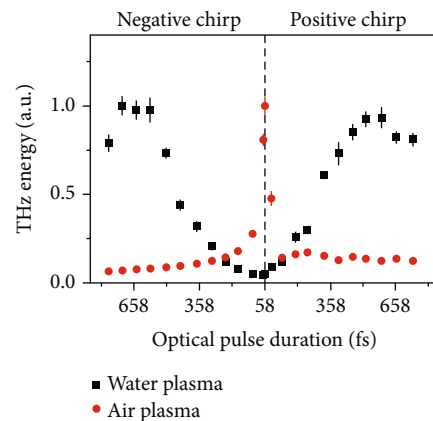

- ■ Water plasma
- ● Air plasma

FIGURE 7: Normalized THz energy with different optical pulse durations [10]. THz signal generated by water plasma prefers an optical excitation with a longer pulse duration. However, the THz wave generation from air plasma is always in favor of the shortest pulse. The optical pulse energy is 0.4 mJ for both cases.
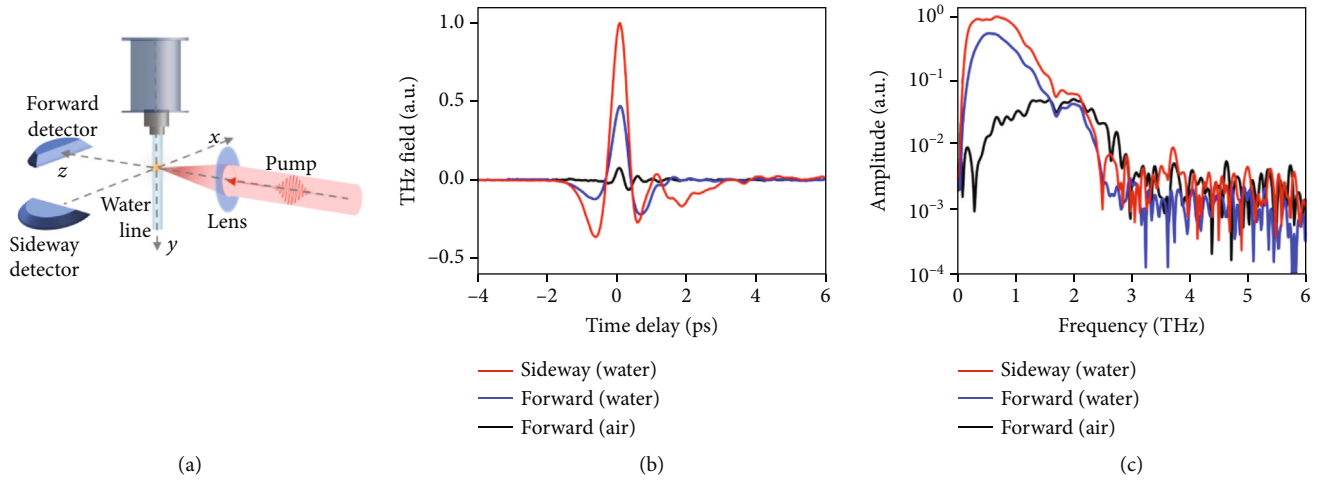
(a)   (b)   (c)

FIGURE 8: Comparison of forward and sideways detection. (a) Setup schematic for forward and sideways detection. The pump beam is along the z-axis. The water line flows in the y direction. Two EO detectors are in the z and x directions. (b) Comparison of THz waveforms. The laser pulse energy is 0.4 mJ. Corresponding spectra are shown in (c).

(a)   (b)   (c)
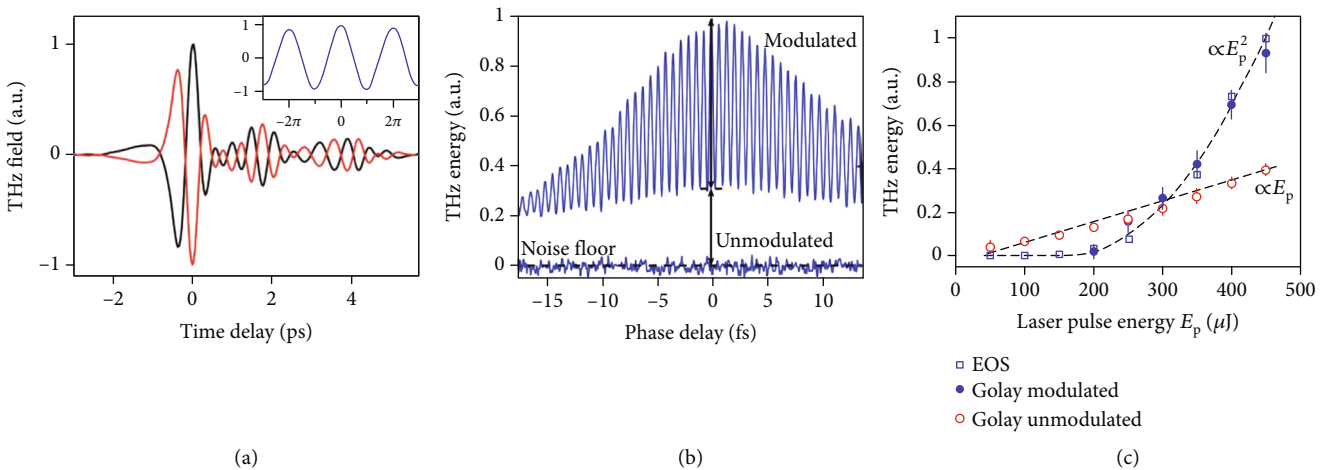
FIGURE 9: THz generation from liquid water under two-color excitation [13]. (a) Two THz waveforms are obtained when the relative phase is π and 2π. Inset: THz electric field as a function of the phase delay. (b) THz wave energy with a tuned phase between 800 nm and 400 nm pulses. The THz energy was monitored by a Golay cell. (c) Normalized THz energy from liquid water as a function of the total laser pulse energy. Blue squares show the THz energy calculated from the temporal integral of the THz waveform measured by EOS. Blue dots indicate modulated THz energy measured by a Golay cell. Red circles present unmodulated THz energy measured by the Golay cell.

shows that the THz waveform from liquid water under two-color excitation is completely flipped over by varying the relative phase of two pump beams by π. The inset plots the THz peak field as a function of the relative phase. Figure 9(b) shows the THz wave energy measured by a Golay cell as a function of the relative optical phase. The noise level is measured when the THz signal is blocked. It is interesting that some of the signals cannot be modulated via the coherent phase control. By calculating from the noise level, the modulated energy is about 70% of the total energy. The modulated and unmodulated THz waves originate from different generation processes. For further exploration, the excitation power dependence for two parts of energy is studied, which is shown in Figure 9(c).

The unmodulated part (red circles) shows a linear dependence on the laser pulse energy. For the modulated part (blue dots), there is a threshold (0.2 mJ), beyond which the signal appears. Its tendency matches a quadratic function above the threshold. This result is also coincident with the result measured from EOS (blue squares). Unlike EOS, the Golay cell can measure both coherent and incoherent signals. Thus, the modulated portion is mainly from the coherent signal resulting from the buildup of bremsstrahlung from electron-atom collisions in the electron acceleration process [41]. In contrast, the unmodulated part may include both coherent and incoherent signals arising from multiple physical processes. For instance, a spatial net charge distribution created by the ponderomotive force radiates THz waves. Since

no threshold is observed for the unmodulated portion, the THz wave emission can also be attributed to that part of the broadband radiation from the combination of thermal bremsstrahlung from electrons and electron-ion recombination. Besides providing an approach to reveal more information about plasma behaviors in liquids, two-color excitation offers an insight into developing a liquid THz source that may have applications in THz nonlinear optics and THz-driven electron acceleration.

4. THz Wave Generation from Other Liquids

The demonstration of THz wave generation from liquid water opens one new avenue for studying THz liquid sources. In contrast to solid material, two distinguished properties are usually used to characterize liquid material. One is viscosity, which depends on the friction among molecules. The other one is surface tension, which relates to the surface that resists force and keeps the liquid together. Besides, ionization threshold, electron density buildup, and THz dispersion are important parameters in the THz generation process. Liquids with different properties emit THz waves with different properties. Measuring the THz wave from different liquids reveals the ultrafast dynamics of the laser-liquid interaction process. In this chapter, we discuss THz wave generation from different liquids.

4.1. Liquid Nitrogen. Compared to liquid water, liquid nitrogen (LN_2) is a good candidate for tests based on the following properties: (1) LN_2 has a surface tension of 8.85 mN/m at −196°C, which is the lowest surface tension to our knowledge except that of liquid helium. For water, it is 71.97 mN/m at 25°C; (2) LN_2 has a much lower viscosity (164 mPa·s at −196°C) than water (889 mPa·s at 25°C); (3) LN_2 is a nonpolar liquid, which has a much lower absorption in THz regime [64]; and (4) the LN_2 liquid phase is at a cryogenic temperature (−196°C). It is interesting to study the different dynamics of liquids with a huge temperature difference under the same optical excitation. THz wave generation from a bulk LN_2 has been demonstrated recently under double-pump geometry with either single- or two-color excitation [16]. The shockwave in LN_2 created by the laser pulse may affect the interaction of the next pulse. To eliminate the influence between laser pulses, a flowing LN_2 line is required. However, the room temperature is much higher than the boiling point of LN_2, which is a challenge to create a flowing line at room temperature.

Actually, when liquid contacts with a hot surface whose temperature is much higher than the boiling point, vaporization creates an insulating layer preventing the liquid from boiling rapidly. This is known as the Leidenfrost effect [65, 66]. Benefiting from this effect, it is possible to create a flowing LN_2 line at an ambient environment. Additionally, another factor concerned is the transient vaporization of LN_2 caused by the pressure difference. Usually, LN_2 is stored in a dewar with a higher pressure inside than the outside. The boiling point highly depends on the pressure and drops with the decrease of the pressure. It means that the boiling point inside the dewar is higher than that outside. If a dewar is con-
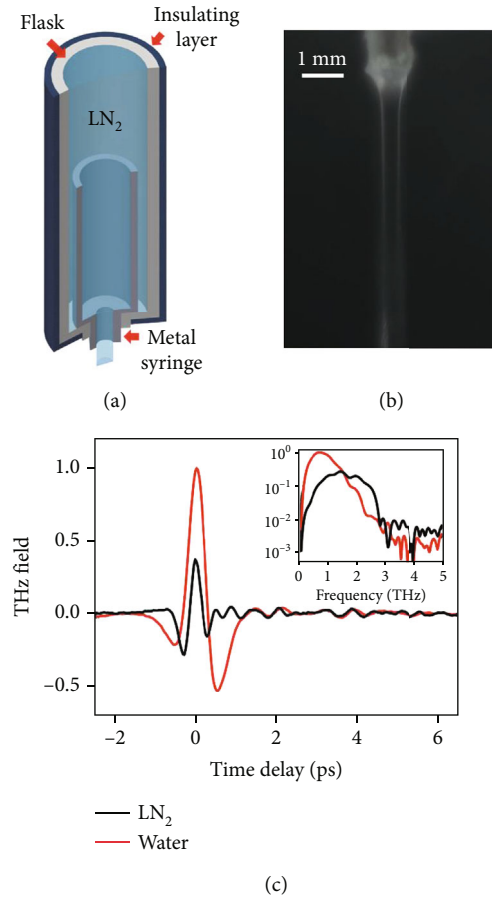

(a)   (b)

(c)

FIGURE 10: THz generation from liquid nitrogen [67]. (a) Diagram of the apparatus for guiding an LN_2 line. By filling it with LN_2, the liquid in the flask prevents the liquid in the syringe transferring heat. (b) A photo of a flowing LN_2 line in an ambient environment. The transparency of the line indicates the liquid phase clearly with a smooth surface. (c) Comparison of THz waveforms from water and LN_2 under the same optical excitation. Inset: corresponding spectra.

nected to a jet directly, a mixture of gas and liquid-phase LN_2 will be ejected out from the jet. To overcome this problem, a phase separator and a custom-designed LN_2 reservoir are needed. As shown in Figure 10(a), the LN_2 reservoir consists of a syringe, a flask, and an insulating layer. The metal syringe is immersed in a flask filled with LN_2 for maintaining the cryogenic temperature. Outside the flask, a thick insulating layer is employed to resist the heat transition between the flask and the ambient environment. The volume of the flask is 600 ml. While filling the flask with LN_2, the syringe is blocked at the beginning until the setup is cooled down. Benefiting from the high thermal conductivity of the metal syringe, the setup reaches the thermal balance quickly. After removing the block, a steady liquid line is formed in the ambient environment. Figure 10(b) is a photo of the flowing LN_2 line. The diameter of the flow is estimated to be 400 ± 5 μm, which is determined by the inner diameter of the syringe needle. The high transparency indicates a smooth surface as well as a stable flow.

TABLE 2: Properties of some liquid metals comparing with water [92–94].

| Metal targets	Melting point (°C)	Surface tension (N/m)	Density (g/cm^3)	Viscosity (Pa·s)	Ionization energy (eV)
Water (at 20°C)	**0**	**0.073**	**0.998**	**0.0010**	**6.5**
Galinstan (at 20°C)	−19.0	0.718	6.440	0.0024	—
Mercury (Hg) (at 20°C)	−38.8	0.487	13.534	0.0015	10.44
Francium (Fr) (at 30°C)	27.0	0.051	1.870	—	4.07
Cesium (Cs) (at 60°C)	28.5	0.675	1.843	0.0058	3.90
Gallium (Ga) (at 53°C)	29.8	0.723	6.080	0.0019	5.98
Rubidium (Rb) (at 100°C)	39.3	0.854	1.460	0.0048	4.18
Phosphorus (P) (at 50°C)	44.0	0.698	1.740	0.0016	10.64
Indium (In) (at 170°C)	156.6	0.558	7.020	0.0019	6.08

(a)   (b)   (c)
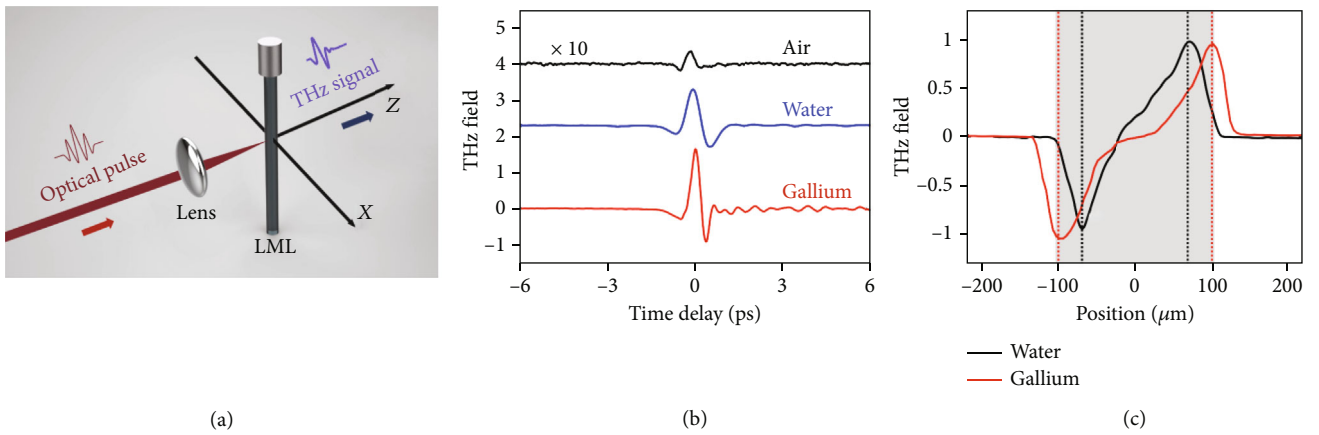
FIGURE 11: THz generation from liquid metal [71]. (a) Schematic of the experimental setup. A two-dimensional translation stage is used to control the position of the x-axis and the z-axis of the liquid metal line. The optical beam propagates along the z-axis. THz emission is measured by a standard electro-optical sampling. (b) Comparison of THz waveforms generated from air, water, and liquid gallium under single-color excitation. The target diameter is 210 μm. The THz signal from air plasma is enlarged by 10 times. (c) Normalized THz field strength plotted as a function of the x-axis position. The dashed lines represent the x-axis position of the maximum THz fields. The gray area shows the diameter of the liquid line.

Figure 10(c) shows the THz waveforms from the LN$_2$ line and a water line under the same experimental conditions. The THz peak field from LN$_2$ is 0.4 times weaker than that from water. However, the THz signal from LN$_2$ shows a shorter pulse duration. By fitting the envelope of the THz signal in the field, the THz signal from LN$_2$ has a pulse duration of 0.6 ps. For the THz signal from water, the THz pulse duration is about 1 ps. The corresponding spectra are shown in the inset. LN$_2$ shows a broader bandwidth with more high-frequency components. There are two possible reasons. First, LN$_2$ has a low absorption in THz regime because it is a non-polar liquid. Additionally, the vaporized N$_2$ keeps purging the system to preserve the high-frequency components. More details of THz wave generation from a flowing LN$_2$ can be found in [67].

4.2. Liquid Gallium.

Metal targets have been considered as great THz radiation sources because of their relatively lower ionization thresholds, which allow THz wave generation by using a lower pump energy compared with water. It would be interesting to discuss the different contributions of electrons excited by laser pulses and free electrons originally existing in the liquid metal in the THz wave generation process. Besides, the surface tension of liquid metal is much higher than that of water, meaning that it is able to form a smoother surface of a flowing liquid line. Because of the chemical stability and physical safety, liquid metal, such as gallium, has been widely used in X-ray generation applications as well [68–70].

Table 2 lists the melting point, surface tension, density, viscosity, and ionization energy of several selected liquid metals. Among those, mercury has the lowest melting point. For the toxicity concern and chemical stability, gallium is more in favor for lab users. The melting point of gallium is 30°C. Using a heater-attached liquid circulating system, a high-quality liquid gallium line can be obtained.

Figure 11(a) shows the schematic of using a liquid gallium line as a THz source. The laser beam is focused by a 2-inch focal length lens on the liquid metal target. The position of the liquid line near the focus is finely controlled by a

two-dimensional translation stage. The diameter of the gallium line is 210 μm. A flowing rate is about 3.8 m/s, which can be controlled by the pump. The forward propagating THz signal is detected, as shown in Figure 11(b). THz signals from both gallium and water lines are much stronger than that from air plasma. The THz signal generated from liquid gallium is 1.7 times stronger in the field than that from water at 35℃. The THz signal from liquid gallium shows a narrower pulse width, indicating that the THz signal from liquid gallium shows a broader bandwidth than that from water. More components at high frequencies are generated, which are also confirmed by their spectra (not shown here).

Figure 11(c) plots the dependence of THz field strength on the x position of the source. The position of the liquid gallium line is scanned across the focus. When x is 0, the optical pump pulse is focused on the center of the gallium line. For a comparison, a similar measurement of water is also plotted. The dashed black and red lines illustrate the x position when the THz fields reach maximum for two liquids, respectively. The measurement clearly shows that the separation between the two maxima of the gallium signal is larger than that of water. The water line has a same diameter as that of the gallium line, which is shown by the gray area. The different sign of the electric field indicates waveforms with opposite polarities. This result shows that the THz signal is generated at the surface of gallium.

The penetration depths of liquid gallium for optical and THz waves are estimated to be 7.7 nm and 60 nm, respectively. Therefore, ionization can only happen at the surface of liquid gallium. Since a longer pulse duration works better for THz wave generation from liquids, enough seed electrons are ionized via multiphoton ionization or tunneling ionization at the front part of the optical pulse. Then, cascade ionization occurs, in which collisions of electrons lead to an exponential increase in the number of electrons. Then, electrons are accelerated by the ponderomotive force as a result of the nonuniform density gradient distribution of plasma. Eventually, the THz wave emits from liquid metal.

Although the flip of THz waveforms from liquid gallium observed by scanning along the x-axis shows similar characteristics with a THz signal from water, the mechanism of THz wave generation from liquid metals likely differs from the generation process of liquid water. Further exploration still needs to be conducted. The THz wave emission pattern, especially the sideways and the backward detection, is an important experiment to understand the THz radiation mechanism. More details of THz generation from a flowing liquid gallium line can be found in [71].

4.3. Liquids with Different Polarity Indices. Molecular polarity describes the separation of positive- and negative-charged particles of a molecule. A polar molecule possesses a dipole contributing to a strong absorption in the THz region [72]. Generally, liquids comprised of nonpolar molecules show a low absorption. The polarity index is a quantitative parameter that defines how polar a liquid is [73]. To investigate the influence of liquid absorption, liquids with different polarity indices are tested. Table 3 lists liquids with different polarity indices. Stronger THz signals are expected

TABLE 3: List of selected liquids with different polarity indices.

Liquid	Polarity	Boiling T (℃)
Alpha-pinene	~0	156
Isooctane	0.1	99
Butyl chloride	1.0	78
p-Xylene	2.5	138
Methylene chloride	3.4	240
Ethyl acetate	4.3	77
Pyridine	5.3	115
Ethanol	6.3	78
Water	9.8	100

(a)

(b)
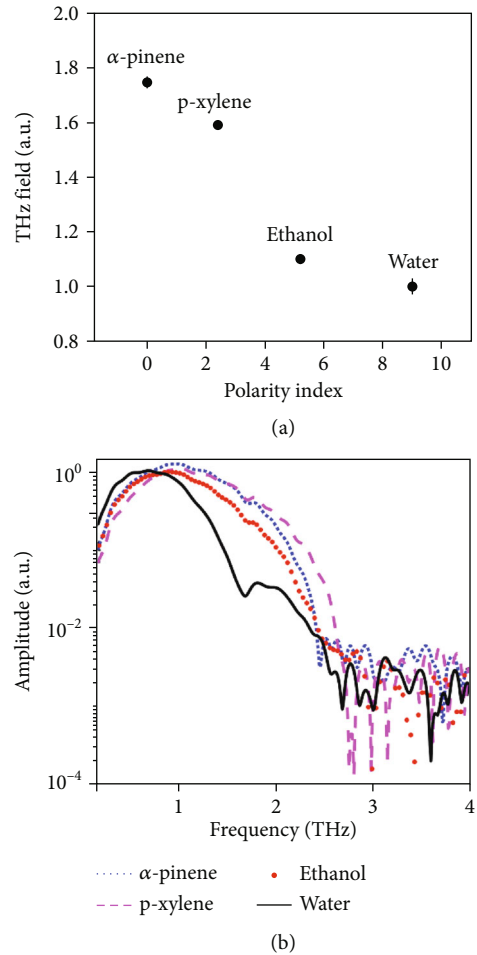
FIGURE 12: THz generation from liquids with different polarity indices. (a) THz fields generated from four liquids, which are α-pinene, p-xylene, ethanol, and water. Their polarity indices are 0, 2.4, 5.2, and 9, respectively. (b) Corresponding spectra.

from liquids with smaller polarity indices for lower absorption.

Figure 12(a) shows the peak-valley values of THz electric fields obtained from four different liquids, which are α-pinene, p-xylene, ethanol, and water. Their polarity indices are 0 (nonpolar), 2.4, 5.2, and 9, respectively. Among these

$\Delta\tau = 3.9$ ps

(a)   (b)   (c)
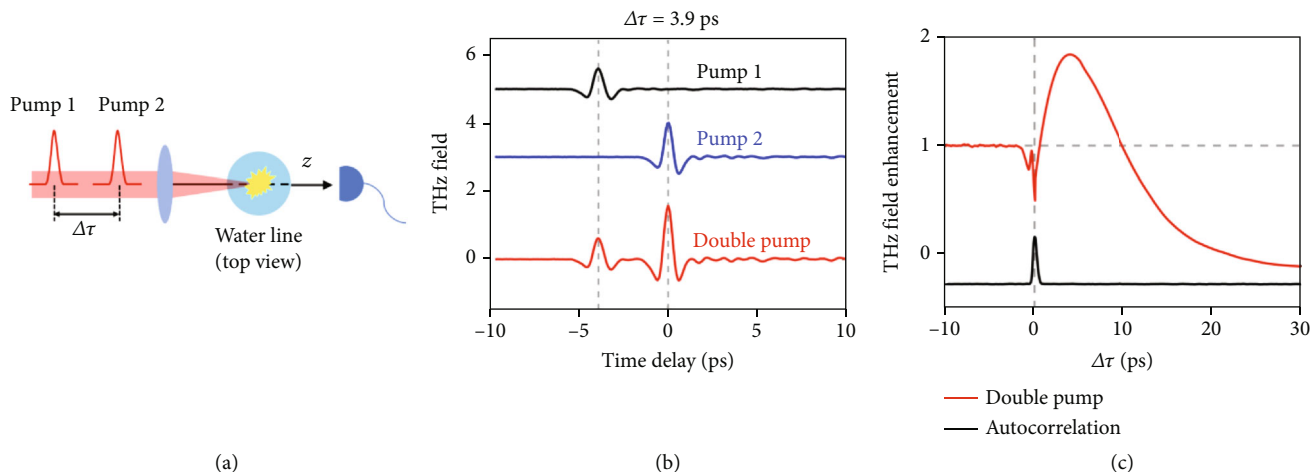
FIGURE 13: THz generation under double-pump excitation [79]. (a) Schematic of double-pump excitation. Two optical pumps propagating collinearly with a certain time delay $\Delta\tau$ are focused on a water line (top view). $\Delta\tau$ is controlled by a delay stage. The THz signal is detected via EOS. (b) THz waveforms generated by pump 1 (black line) and pump 2 (blue line). The bottom red line shows the waveform generated by two pumps when $\Delta\tau$ is 3.9 ps. (c) The red line shows the dynamic enhancement of the THz peak field versus $\Delta\tau$. The black line plots the autocorrelation signal of the two pumps, from which the 0 timing is determined. $\Delta\tau > 0$ means that the pump 1 ionizes the target first.

liquids, α-pinene offers the strongest THz signal, which is about 1.8 times stronger in the field than that from water under the identical experimental conditions (liquid line diameter, laser pulse energy, laser pulse duration, F/#, etc.). Figure 12(b) plots the comparison in the corresponding spectra. Water generates the THz signal with much less high-frequency components. This could be the stronger absorption of water in the high-THz frequency region. Although ethanol exhibits a similar peak-valley value of the THz field to water, it generates more high-frequency THz waves. The widest bandwidth is achieved by p-xylene while the highest amplitude is obtained by α-pinene. Even though there are some other factors that may also influence the THz radiation from different liquids such as refractive index, surface tension, and viscosity, the result shows that molecular polarity or absorption coefficient of liquid plays an important role in the generation process of THz waves both in the peak field and spectrum bandwidth.

5. THz Wave Enhancement under Double-Pump Optical Excitation

Double-pump optical excitation is a technology to improve the generation efficiency via the nonstationary nonlinearity enhancement, in which two pump beams with a certain time delay are used for excitation. Usually, the first pump ionizing target is relatively weaker in power than the second pulse. The time delay is optimized to get the highest signal. To boost the generation efficiency for different wavelengths, the time delay may be varied greatly. The double-pump excitation was originally a practical strategy to enhance the X-ray generation efficiency from liquids. Berglund et al. reported an eight-times increase in the intensity of extreme-ultraviolet emission by using ethanol droplets as targets for a double-pump excitation [74]. Additionally, Anand et al. reported a 68-times increase in the intensity of hard X-ray emission

from methanol droplets irradiated by double-pulsed femtosecond laser pulses with a delay time of 10 ns [75]. Double-pump excitation is also studied in THz wave generation [16, 76–79]. Recently, THz generation enhancement by several orders of magnitude in power is observed from gallium droplets under double pump excitation [80].

Figure 13(a) shows a schematic of double-pump excitation on a liquid line for THz wave generation in top view. Two pump beams propagating collinearly with a time delay $\Delta\tau$ are focused on the liquid line. The position of the liquid line is precisely controlled by a two-dimensional stage in the $x - y$ plane. When the liquid line moves across the focus, the incidence angle of two pumps is varied accordingly because of the curved surface of the liquid line. THz signal generated from liquid water is shown in Figure 13(b). The top two waveforms show the results from two individual pumps. The time delay $\Delta\tau$ between two pump beams is reflected on the time delay of THz waveforms, which is 3.9 ps. This time delay is longer than the pulse duration and smaller than the lifetime of the photoexcited electrons (nanosecond level). Pump 2 with greater pulse energy produces a stronger THz signal. Two THz waveforms keep the same shape indicating a good overlap of the two pump beams. The bottom waveform in Figure 13(b) shows the result of the double-pump excitation. The THz signal generated by pump 2 is enhanced because of the existence of the ionization by pump 1. The THz waveform keeps being the same, which indicates that the spectral components are enhanced equally.

The temporal dependence of the THz field enhancement on the time delay is shown in Figure 13(c). By varying $\Delta\tau$, the peak field of the THz waveform generated by pump 2 is recorded. The zero timing of $\Delta\tau$ is determined by the peak of the autocorrelation signal (black line) of two pump beams. The enhanced dynamic (red line) results from either the interaction of two plasmas produced by two pump beams or the influence of the first-produced plasma on the pump

2. It could not be the direct interaction of two pump beams because the enhancement happens in a picosecond time scale, which is much longer than that of two-pulse interaction (~100 fs). As shown in the plot, when $\Delta\tau < 0$, pump 2 arrives at the water line first and generates a THz signal. Pump 1 comes later and has no influence on it. Therefore, the THz signal keeps the same peak value (normalized to 1) until pump 1 catches up on pump 2. The THz signal starts to change when two pump beams temporally overlap with each other. The enhancement gradually increases up to the maximum. A maximum enhancement of 1.8 times in THz field is observed in this case. Additionally, the enhancement lasts a long time. It is noteworthy that the time delay supporting the enhancement is over 10 ps. Eventually, the THz field decreases because of the absorption of the first plasma. More details can be found in [79]. For the double-pump excitation, one possible reason of the enhancement is that the preexisting plasma provides more initial electrons for the cascade ionization. Under single-color excitation, the multiphoton or tunneling ionization processes give rise to the initial ionization of the target at the front of the optical pulse. Instead, under double-pump excitation, the preionized plasma generated by the first pulse provides a higher electron density. By changing the power ratio and polarizations of two pump beams, the enhancement can be optimized. Currently, the energy conversion is about 10^{-5} under the double-pump excitation, which is one order higher than that of the single-color excitation.

6. Ultrafast Dynamics in Liquids Excited by Intense THz Waves

When a strong enough electric field is applied to an isotropic media, birefringence is created, which is well-known as the Kerr effect [81, 82]. As the development of THz sources in recent decades, it was realized that the intense THz pulse induces the transient Kerr effect, as known as the THz Kerr effect (TKE) [83]. This finding offers a new method of investigating the ultrafast evolution of the Kerr effect in a picosecond timescale. The hydrogen bond vibrations as well as other molecular motions in aqueous solutions could be characterized in the THz range, which play an important role in understanding the thermodynamic properties of liquids [84]. By employing the technique of the THz Kerr effect, the low-frequency molecular dynamics is able to be studied experimentally.

Figure 14(a) shows the diagram of a THz Kerr effect setup. An intense THz pulse with the maximum peak electric field strength of 14.9 MV/cm is focused on a gravity-driven, free-standing liquid film. The liquid samples could be pure water or aqueous salt solutions with different concentrations. One optical beam propagated collinearly with a THz beam is measured in a balanced photodetector. The THz-induced birefringence is recorded by measuring the polarization change of the optical beam. Figure 14(b) shows a bipolar THz Kerr effect response with significant oscillation characteristics in liquid water. The response linearly increases with the peak intensity of THz pulse, indicating that the Kerr effect is dominant here. The broadband THz pulse covers two
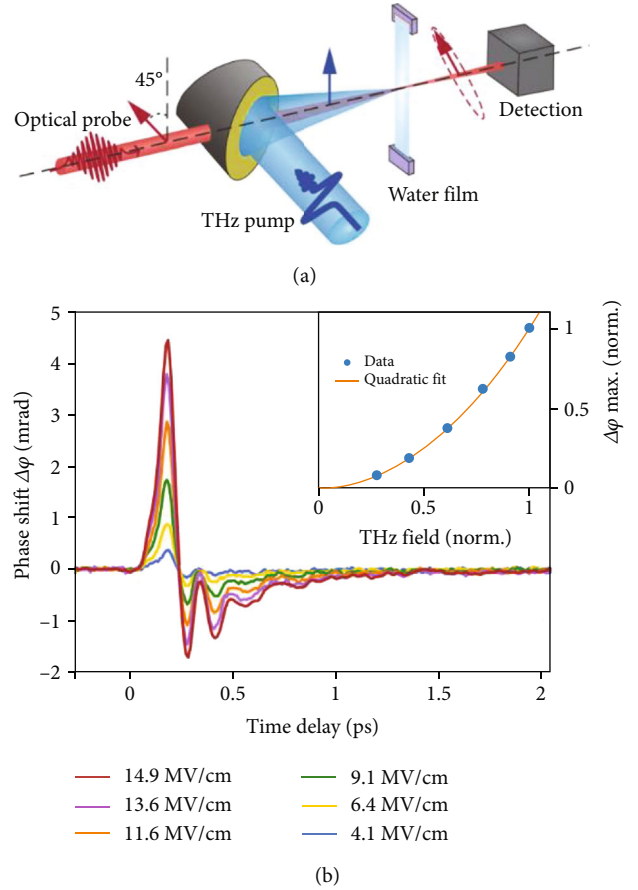

(a)

(b)

FIGURE 14: Terahertz Kerr effect (TKE) in a water film [85]. (a) Diagram of the experimental setup. An intense THz pulse generated from an organic crystal DAST (4-N, N-dimethylamino-$4'$-N$'$-methyl-stilbazolium tosylate) is focused onto a free-standing water film. The THz field-induced Kerr effect is detected by an optical probe. (b) TKE with different THz peak field strengths. Inset: THz field strength dependence.

modes of intermolecular motions, which are hydrogen bond bending and stretching vibrations, respectively. The positive signal caused by hydrogen bond stretching vibration and the negative signal caused by hydrogen bond bending vibration indicate that the polarizability perturbation of water presents competing contributions under bending and stretching conditions. More details can be found in [85].

To simulate the molecular motions, the Lorentz dynamic equation is adopted in the model, which is based on the perturbation in the dielectric tensor caused by the intermolecular vibration modes. The resulting polarizability anisotropy can be expressed by the refractive index associated with the dielectric susceptibility [85, 86]:

$$\sum_{i=1,2} \Delta n_i = \frac{1}{2\varepsilon_0 n_0}\left[\varepsilon_y - \frac{1}{2}\left(\varepsilon_x + \varepsilon_z\right)\right] = \frac{1}{2n_0}\left(\frac{\partial\chi_\parallel}{\partial Q_s}q_2 - \frac{\partial\chi_\perp}{\partial Q_b}q_1\right),$$

(1)

where ε_0 is the vacuum dielectric constant and n_0 is the refractive index of liquid water. q_1 and q_2 represent the
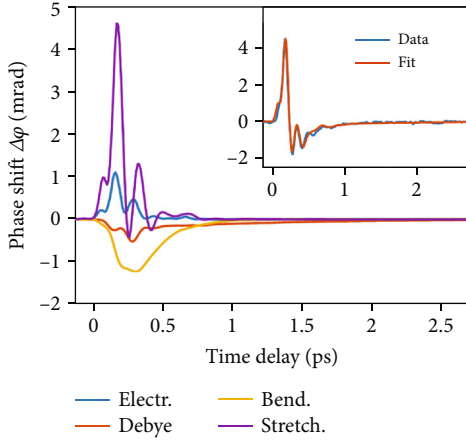
FIGURE 15: Simulation of the TKE response [85]. The simulation results of the TKE response in the time domain for the electronic (Electr.), Debye relaxation (Debye), hydrogen bond bending vibration (Bend.), and hydrogen bond stretching vibration (Stretch.) contributions. Inset: a comparison between the sum of the fitted contributions and the measured data.

anisotropic perturbations caused by hydrogen bond bending and stretching vibrations, respectively. Q_b and Q_s represent the bending and stretching vibration amplitudes, respectively, of a single hydrogen bond unit. $\chi_{\parallel}$ and $\chi_{\perp}$ represent the perturbations of the dielectric susceptibilities parallel and perpendicular to the hydrogen bond direction caused by the intermolecular modes. These two intermolecular motions result in opposite birefringence contributions to the total refractive index, i.e., $\Delta n_1 < 0$, $\Delta n_2 > 0$.

In addition, q_i satisfies the Lorentz dynamic model, which describes the motion of the damped harmonic oscillator [87, 88]:

$$\frac{\partial^2 q_i(t)}{\partial t^2} + \gamma_i \frac{\partial q_i(t)}{\partial t} + \omega_i^2 q_i(t) = a_i E^2(t), \quad (i = 1, 2), \quad (2)$$

where γ_i, ω_i represent the damping coefficient and inherent frequency, respectively, with values of $\gamma_1 = 115\,\mathrm{cm}^{-1}$, $\gamma_2 = 165\,\mathrm{cm}^{-1}, \omega_1 = 60\,\mathrm{cm}^{-1}$, and $\omega_2 = 190\,\mathrm{cm}^{-1}$. Here, $a_i = \beta_i(\mu_0^2/3\sqrt{2}k_B T m)$ represents the coupling factor between the square of the THz pump electric field and the driving term in equation (2). We use the above model to decompose and simulate the experimental data in the time domain, as shown in Figure 15. The data can be decomposed into (i) positive responses with electronic (Electr.) and hydrogen bond stretching (Stretch.) contributions and (ii) negative responses with Debye relaxation (Debye) and hydrogen bond bending (Bend.) contributions.

For ionic aqueous solutions, the TKE signals of NaCl, NaBr, and NaI solutions in different concentrations are measured, as shown in Figure 16(a). Accordingly, the amplitude and shape of the THz Kerr effect responses vary with exchanging anions when the counter ion is Na$^+$. These signals are also theoretically decomposed into the weak electronic responses and different molecular motion modes [89], as show in Figure 16(b). For the bending mode, the
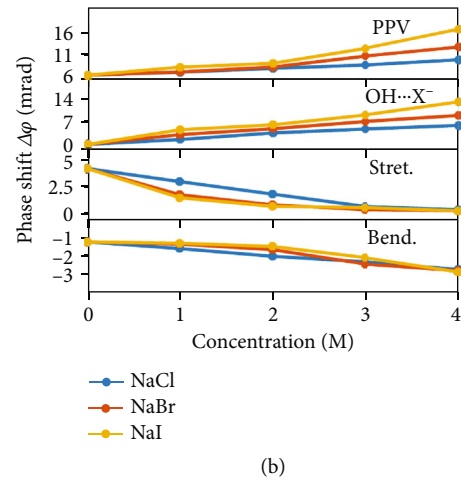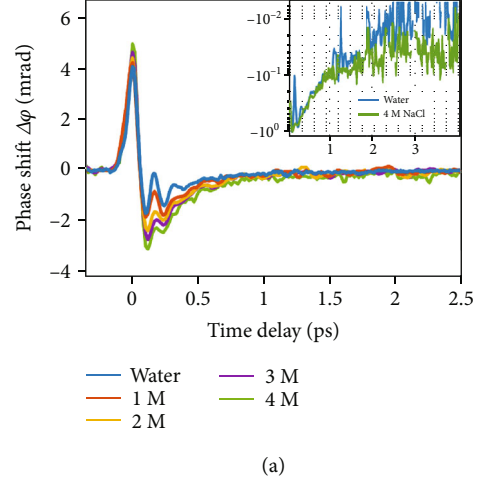

(a)

(b)

FIGURE 16: Terahertz Kerr effect response on different concentrations [89]. (a) TKE responses of water and NaCl solutions in different concentrations. Inset: an enlarged logarithmic view of the negative polarity responses. (b) The upper panel shows the measured peak-to-peak values (PPV) of TKE responses for NaCl, NaBr, and NaI solutions in different concentrations. The other panels show the extracted maximum values of TKE responses induced by OH… X$^-$ hydrogen bond vibration (OH…X$^-$), the hydrogen bond stretching modes (Stret.), and the hydrogen bond bending (Bend.).

amplitude of negative polarity response gradually increases as the concentration increases. However, the damping coefficient and inherent frequency do not change significantly in this overdamped oscillation system. For the stretching mode, the positive polarity response gradually decreases along with the weakening of oscillation characteristics as the concentration increases, because the addition of ions dilutes the hydrogen bond density and destroys the water network structure. However, as the concentration increases, the positive polarity response increases, indicating that the interaction of ions with water provides a larger positive polarity response than that from the water-water hydrogen bond stretching mode. The enhanced positive response originated from the special hydrogen bond vibration formed between the anions and the water molecules (OH…X$^-$, X$^-$: Cl$^-$, Br$^-$, and I$^-$) [90, 91], and the addition of anions will greatly reduce the water-water hydrogen bond vibration. As the ion

TABLE 4: Comparison between THz generation from air and water.

	Air	Water
Optimal optical pulse duration	Shortest	Subpicosecond
Central THz frequency	$1 \sim 1.5$ THz	$0.5 \sim 1$ THz
THz signal bandwidth	$1 \sim 1.5$ THz	$0.5 \sim 1$ THz
Two-color enhancement in power	$\sim 10^6$	$\sim 10^2$
Fluorescence and white light	Relatively week	Much brighter
Sideways signal (2 in lens is used)	No measurable signal	Strong sideways signal

concentration increases, the low-frequency molecular motion in water is gradually dominated by ion-water hydrogen bond motion.

For the OH…X^- hydrogen bond vibration mode, the THz Kerr effect response increases significantly with the increase of concentration for all the three kinds of solutions. In particular, the NaI solution exhibits higher anisotropy response at the same concentration. This is because for the low surface charge density of anion (such as I^-), the formed OH…X^- hydrogen bond has a relatively long bond length and low binding energy [91]. In addition, the center frequency of 3.9 THz of the THz pulse is closer to the inherent frequency of the OH…I^- hydrogen bond vibration. Therefore, an enhanced dipole moment and a greater polarizability anisotropy under OH…I^- hydrogen bond vibration mode could be achieved with the resonant THz electric field excitation.

The THz Kerr effect measurement directly observes the ultrafast temporal evolution of intermolecular hydrogen bond dynamics in aqueous solutions at the subpicosecond scale. The THz Kerr effect technique helps us explore the low-frequency dynamics and successfully obtain the THz Kerr effect responses in various aqueous solutions, such as pure water and halide anion aqueous solutions. The results provide an experimental basis for further insight into the ultrafast evolution of transient structures in complex aqueous solutions. We believe that the THz Kerr effect method can also be applied to detect the physical mechanisms of the complex interaction of reagents with solvent water molecules, which can provide the further insight into the effects of the hydrogen bond network on the biochemical reaction and the related structural dynamics in water environment.

7. Outlook

Currently, the THz field generated from liquid under single-color excitation is 2 orders higher than that from single-color air plasma. A detailed comparison between THz wave generation from air and water is shown in Table 4. It should be noted that this comparison is only valid under certain experimental conditions (2-inch focal length lens, 0.4 mJ pulse energy, and 60 fs Fourier transform limited pulse). Broadband THz wave generation from liquid is a new research topic; detailed systematic theoretical and experimental studies are necessary. The optimal conditions for the maximum generation efficiency are underexplored. Further experiments

include target geometry design, laser pulse shaping, target material testing, and external field modulating.

Furthermore, one of the most interesting projects is to study THz wave generation from superfluid such as ^{4}He, which flows with no viscosity, and its thermal conductivity increases by a factor of $\sim 10^6$ for the temperature at the λ point. This causes heat in the liquid to be transferred to its surface so quickly that vaporization takes place only at the free surface of the liquid. Thus, there are no gas bubbles in the body of the superfluid ^{4}He. Therefore, the superfluid ^{4}He serves as a perfect system for the optical study on the laser-matter interaction by focusing laser beam in the liquid.

THz liquid photonics provides a new platform for the THz community, which offers an opportunity for developing liquid THz sources and exploring the light-liquid interaction. THz wave generation from liquids presents its specialties and superiorities compared to the gas and solid targets, which should be further studied to draw a thorough picture for the laser-induced ionization process in liquid. All efforts in this topic will help pave the way toward developing intense liquid THz sources and offer a better insight into the laser-liquid interaction process. The future of THz liquid photonics is hardly fully predictable, but it is certainly bright.

Data Availability

Data is available upon reasonable request.

Conflicts of Interest

The authors declare that there is no conflict of interest regarding the publication of this article.

Acknowledgments

References

[1] H. Hamster, A. Sullivan, S. Gordon, W. White, and R. W. Falcone, "Subpicosecond, electromagnetic pulses from intense laser-plasma interaction," *Physical Review Letters*, vol. 71, no. 17, pp. 2725–2728, 1993.

[2] H. Hamster, A. Sullivan, S. Gordon, and R. W. Falcone, "Short-pulse terahertz radiation from high-intensity-laser-produced plasmas," *Physical Review E*, vol. 49, no. 1, pp. 671–677, 1994.

[3] D. J. Cook and R. M. Hochstrasser, "Intense terahertz pulses by four-wave rectification in air," *Optics Letters*, vol. 25, no. 16, pp. 1210–1212, 2000.

[4] M. Clerici, M. Peccianti, B. E. Schmidt et al., "Wavelength scaling of terahertz generation by gas ionization," *Physical Review Letters*, vol. 110, no. 25, p. 253901, 2013.

[5] X. Xie, J. Dai, and X. C. Zhang, "Coherent control of THz wave generation in ambient air," *Physical Review Letters*, vol. 96, no. 7, p. 075005, 2006.

[6] J. Dai, J. Liu, and X. C. Zhang, "Terahertz wave air photonics: terahertz wave generation and detection with laser-induced gas plasma," *IEEE Journal of Selected Topics in Quantum Electronics*, vol. 17, no. 1, pp. 183–190, 2011.

[7] F. Jahangiri, M. Hashida, T. Nagashima, S. Tokita, M. Hangyo, and S. Sakabe, "Intense terahertz emission from atomic cluster plasma produced by intense femtosecond laser pulses," *Applied Physics Letters*, vol. 99, no. 26, p. 261503, 2011.

[8] T. Nagashima, H. Hirayama, K. Shibuya et al., "Terahertz pulse radiation from argon clusters," *Optics Express*, vol. 17, no. 11, pp. 8907–8912, 2009.

[9] K. Mori, M. Hashida, T. Nagashima et al., "Directional linearly polarized terahertz emission from argon clusters irradiated by noncollinear double-pulse beams," *Applied Physics Letters*, vol. 111, no. 24, p. 241107, 2017.

[10] Q. Jin, Y. E, K. Williams, J. Dai, and X. C. Zhang, "Observation of broadband terahertz wave generation from liquid water," *Applied Physics Letters*, vol. 111, no. 7, p. 071103, 2017.

[11] I. Dey, K. Jana, V. Y. Fedorov et al., "Highly efficient broadband terahertz generation from ultrashort laser filamentation in liquids," *Nature Communications*, vol. 8, no. 1, p. 1184, 2017.

[12] E. Yiwen, Q. Jin, A. Tcypkin, and X. C. Zhang, "Terahertz wave generation from liquid water films via laser-induced breakdown," *Applied Physics Letters*, vol. 113, no. 18, p. 181103, 2018.

[13] Q. Jin, J. M. Dai, E. Yiwen, and X. C. Zhang, "Terahertz wave emission from a liquid water film under the excitation of asymmetric optical fields," *Applied Physics Letters*, vol. 113, no. 26, p. 261101, 2018.

[14] A. N. Tcypkin, E. A. Ponomareva, S. E. Putilin et al., "Flat liquid jet as a highly efficient source of terahertz radiation," *Optics Express*, vol. 27, no. 11, p. 15485, 2019.

[15] L.-L. Zhang, W.-M. Wang, T. Wu et al., "Strong terahertz radiation from a liquid-water line," *Physical Review Applied*, vol. 12, no. 1, p. 014005, 2019.

[16] A. V. Balakin, J.-L. Coutaz, V. A. Makarov et al., "Terahertz wave generation from liquid nitrogen," *Photonics Research*, vol. 7, no. 6, p. 678, 2019.

[17] A. Gopal, P. Singh, S. Herzer et al., "Characterization of 700 μJ T rays generated during high-power laser solid interaction," *Optics Letters*, vol. 38, no. 22, pp. 4705–4707, 2013.

[18] G. Liao, Y. Li, H. Liu et al., "Multimillijoule coherent terahertz bursts from picosecond laser-irradiated metal foils," *Proceedings of the National Academy of Sciences*, vol. 116, no. 10, pp. 3994–3999, 2019.

[19] A. Woldegeorgis, T. Kurihara, M. Almassarani et al., "Multi-MV/cm longitudinally polarized terahertz pulses from laser–thin foil interaction," *Optica*, vol. 5, no. 11, p. 1474, 2018.

[20] G.-Q. Liao, Y.-T. Li, Y.-H. Zhang et al., "Demonstration of coherent terahertz transition radiation from relativistic laser-solid interactions," *Physical Review Letters*, vol. 116, no. 20, p. 205003, 2016.

[21] A. W. Miziolek, V. Palleschi, and I. Schechter, *Laser Induced Breakdown Spectroscopy*, Cambridge University Press, 2006.

[22] F. Anabitarte, A. Cobo, and J. M. Lopez-Higuera, "Laser-induced breakdown spectroscopy: fundamentals, applications, and challenges," *ISRN Spectroscopy*, vol. 2012, Article ID 285240, 12 pages, 2012.

[23] B. Kearton and Y. Mattley, "Sparking new applications," *Nature Photonics*, vol. 2, no. 9, pp. 537–540, 2008.

[24] S. Corde, K. Ta Phuoc, G. Lambert et al., "Femtosecond x rays from laser-plasma accelerators," *Reviews of Modern Physics*, vol. 85, no. 1, pp. 1–48, 2013.

[25] J. Yoshii, C. H. Lai, T. Katsouleas, C. Joshi, and W. B. Mori, "Radiation from Cerenkov wakes in a magnetized plasma," *Physical Review Letters*, vol. 79, no. 21, pp. 4194–4197, 1997.

[26] D. Kuk, Y. J. Yoo, E. W. Rosenthal, N. Jhajj, H. M. Milchberg, and K. Y. Kim, "Generation of scalable terahertz radiation from cylindrically focused two-color laser pulses in air," *Applied Physics Letters*, vol. 108, no. 12, p. 121106, 2016.

[27] T. I. Oh, Y. J. Yoo, Y. S. You, and K. Y. Kim, "Generation of strong terahertz fields exceeding 8 MV/cm at 1 kHz and real-time beam profiling," *Applied Physics Letters*, vol. 105, no. 4, p. 041103, 2014.

[28] X. C. Zhang, A. Shkurinov, and Y. Zhang, "Extreme terahertz science," *Nature Photonics*, vol. 11, no. 1, pp. 16–18, 2017.

[29] J. Liu and X. C. Zhang, "Terahertz-radiation-enhanced emission of fluorescence from gas plasma," *Physical Review Letters*, vol. 103, no. 23, p. 235002, 2009.

[30] J. Liu, J. Dai, S. L. Chin, and X. C. Zhang, "Broadband terahertz wave remote sensing using coherent manipulation of fluorescence from asymmetrically ionized gases," *Nature Photonics*, vol. 4, no. 9, pp. 627–631, 2010.

[31] B. Clough, J. Liu, and X. C. Zhang, ""All air-plasma" terahertz spectroscopy," *Optics Letters*, vol. 36, no. 13, pp. 2399–2401, 2011.

[32] J. Liu, B. Clough, and X. C. Zhang, "Enhancement of photoacoustic emission through terahertz-field-driven electron motions," *Physical Review E*, vol. 82, no. 6, p. 066602, 2010.

[33] B. Clough, J. Liu, and X. C. Zhang, "Laser-induced photoacoustics influenced by single-cycle terahertz radiation," *Optics Letters*, vol. 35, no. 21, pp. 3544–3546, 2010.

[34] F. Buccheri and X.-C. Zhang, "Terahertz emission from laser-induced microplasma in ambient air," *Optica*, vol. 2, no. 4, p. 366, 2015.

[35] C. D'Amico, A. Houard, M. Franco et al., "Conical forward THz emission from femtosecond-laser-beam filamentation in air," *Physical Review Letters*, vol. 98, no. 23, p. 235002, 2007.

[36] J. Dai, N. Karpowicz, and X. C. Zhang, "Coherent polarization control of terahertz waves generated from two-color laser-induced gas plasma," *Physical Review Letters*, vol. 103, no. 2, p. 023001, 2009.

[37] H. Wen and A. M. Lindenberg, "Coherent terahertz polarization control through manipulation of electron trajectories," *Physical Review Letters*, vol. 103, no. 2, p. 023902, 2009.

[38] K.-Y. Kim, "Generation of coherent terahertz radiation in ultrafast laser-gas interactions," *Physics of Plasmas*, vol. 16, no. 5, p. 056706, 2009.

[39] K.-Y. Kim, J. H. Glownia, A. J. Taylor, and G. Rodriguez, "Terahertz emission from ultrafast ionizing air in symmetry-broken laser fields," *Optics Express*, vol. 15, no. 8, pp. 4577–4584, 2007.

[40] K.-Y. Kim, A. Taylor, J. Glownia, and G. Rodriguez, "Coherent control of terahertz supercontinuum generation in ultrafast laser- gas interactions," *Nature Photonics*, vol. 2, no. 10, pp. 605–609, 2008.

[41] N. Karpowicz and X.-C. Zhang, "Coherent terahertz echo of tunnel ionization in gases," *Physical Review Letters*, vol. 102, no. 9, p. 093001, 2009.

[42] J. Dai, X. Xie, and X. C. Zhang, "Detection of broadband terahertz waves with a laser-induced plasma in gases," *Physical Review Letters*, vol. 97, no. 10, p. 103903, 2006.

[43] N. Karpowicz, J. Dai, X. Lu et al., "Coherent heterodyne time-domain spectrometry covering the entire "terahertz gap"," *Applied Physics Letters*, vol. 92, no. 1, p. 011131, 2008.

[44] Q. Wu and X. C. Zhang, "7 terahertz broadband GaP electro-optic sensor," *Applied Physics Letters*, vol. 70, no. 14, pp. 1784–1786, 1997.

[45] Y. Chen, M. Yamaguchi, M. Wang, and X. C. Zhang, "Terahertz pulse generation from noble gases," *Applied Physics Letters*, vol. 91, no. 25, p. 251116, 2007.

[46] G. Rodriguez, "Scaling behavior of ultrafast two-color terahertz generation in plasma gas targets: energy and pressure dependence," *Optics Express*, vol. 18, no. 14, p. 15130, 2010.

[47] S. L. Chin, T. J. Wang, C. Marceau et al., "Advances in intense femtosecond laser filamentation in air," *Laser Physics*, vol. 22, no. 1, pp. 1–53, 2012.

[48] A. Sagisaka, H. Daido, S. Nashima et al., "Simultaneous generation of a proton beam and terahertz radiation in high-intensity laser and thin-foil interaction," *Applied Physics B*, vol. 90, no. 3-4, pp. 373–377, 2008.

[49] S. Feng, L. Dong, T. Wu et al., "Terahertz wave emission from water lines," *Chinese Optics Letters*, vol. 18, no. 2, p. 023202, 2020.

[50] Q. Jin, E. Yiwen, S. Gao, and X. C. Zhang, "Preference of subpicosecond laser pulses for terahertz wave generation from liquids," *Advanced Photonics*, vol. 2, no. 1, 2020.

[51] A. Ismagilov, E. Ponomareva, M. Zhukova, S. E. Putilin, B. A. Nasedkin, and A. N. Tcypkin, "Liquid jet-based broadband terahertz radiation source," *Optical Engineering*, vol. 60, no. 8, 2021.

[52] F. Williams, S. Varma, and S. Hillenius, "Liquid water as a lone-pair amorphous semiconductor," *The Journal of Chemical Physics*, vol. 64, no. 4, pp. 1549–1554, 1976.

[53] D. N. Nikogosyan, A. A. Oraevsky, and V. I. Rupasov, "Two-photon ionization and dissociation of liquid water by powerful laser UV radiation," *Chemical Physics*, vol. 77, no. 1, pp. 131–143, 1983.

[54] R. A. Crowell and D. M. Bartels, "Multiphoton ionization of liquid water with 3.0–5.0 eV photons," *The Journal of Physical Chemistry*, vol. 100, no. 45, pp. 17940–17949, 1996.

[55] L. Malmqvist, L. Rymell, and H. M. Hertz, "Droplet-target laser-plasma source for proximity x-ray lithography," *Applied Physics Letters*, vol. 68, no. 19, pp. 2627–2629, 1996.

[56] M. Berglund, L. Rymell, H. M. Hertz, and T. Wilhein, "Cryogenic liquid-jet target for debris-free laser-plasma soft x-ray generation," *Review of Scientific Instruments*, vol. 69, no. 6, pp. 2361–2364, 1998.

[57] K. M. George, J. T. Morrison, S. Feister et al., "High-repetition-rate (≥ kHz) targets and optics from liquid microjets for high-intensity laser–plasma interactions," *High Power Laser Science and Engineering*, vol. 7, article E50, 2019.

[58] L. Thrane, R. H. Jacobsen, P. Uhd Jepsen, and S. R. Keiding, "THz reflection spectroscopy of liquid water," *Chemical Physics Letters*, vol. 240, no. 4, pp. 330–333, 1995.

[59] C. Ronne, L. Thrane, P. O. Åstrand, A. Wallqvist, K. V. Mikkelsen, and S. R. Keiding, "Investigation of the temperature dependence of dielectric relaxation in liquid water by THz reflection spectroscopy and molecular dynamics simulation," *The Journal of Chemical Physics*, vol. 107, no. 14, pp. 5319–5331, 1997.

[60] T. Wang, P. Klarskov, and P. U. Jepsen, "Ultrabroadband THz time-domain spectroscopy of a free-flowing water film," *IEEE Transactions on Terahertz Science and Technology*, vol. 4, no. 4, pp. 425–431, 2014.

[61] S. L. Chin, *Femtosecond Laser Filamentation*, Springer, 2010.

[62] S. Stumpf, E. Ponomareva, A. Tcypkin, S. Putilin, A. Korolev, and S. Kozlov, "Temporal field and frequency spectrum of intense femtosecond radiation dynamics in the process of plasma formation in a dielectric medium," *Laser Physics*, vol. 29, no. 12, p. 124014, 2019.

[63] E. A. Ponomareva, S. A. Stumpf, A. N. Tcypkin, and S. A. Kozlov, "Impact of laser-ionized liquid nonlinear characteristics on the efficiency of terahertz wave generation," *Optics Letters*, vol. 44, no. 22, pp. 5485–5488, 2019.

[64] J. Samios, U. Mittag, and T. Dorfmüller, "The far infrared absorption spectrum of liquid nitrogen," *Molecular Physics*, vol. 56, no. 3, pp. 541–556, 1985.

[65] J. G. Leidenfrost, *De aquae communis nonnullis qualitatibus tractatus*, Ovenius, 1756.

[66] B. S. Gottfried, C. J. Lee, and K. J. Bell, "The Leidenfrost phenomenon: film boiling of liquid droplets on a flat plate," *International Journal of Heat and Mass Transfer*, vol. 9, no. 11, pp. 1167–1188, 1966.

[67] E. Yiwen, Y. Cao, F. Ling, and X. C. Zhang, "Flowing cryogenic liquid target for terahertz wave generation," *AIP Advances*, vol. 10, no. 10, p. 105119, 2020.

[68] O. Hemberg, M. Otendal, and H. M. Hertz, "Liquid-metal-jet anode electron-impact x-ray source," *Applied Physics Letters*, vol. 83, no. 7, pp. 1483–1485, 2003.

[69] D. H. Larsson, P. A. Takman, U. Lundström, A. Burvall, and H. M. Hertz, "A 24 keV liquid-metal-jet x-ray source for biomedical applications," *Review of Scientific Instruments*, vol. 82, no. 12, p. 123701, 2011.

[70] E. Espes, T. Andersson, F. Bjornsson et al., "Liquid-metal-jet x-ray tube technology and tomography applications," *Digital Imaging XVIII*, p. 7, 2015.

[71] Y. Cao, Y. E, P. Huang, and X. C. Zhang, "Broadband terahertz wave emission from liquid metal," vol. 117, Tech. Rep. 4, Applied Physics Letters, 2020.

[72] Y.-S. Lee, *Principles of Terahertz Science and Technology*, Springer Science & Business Media, 2009.

[73] L. R. Snyder, "Classification of the solvent properties of common liquids," *Journal of Chromatography A*, vol. 92, no. 2, pp. 223–230, 1974.

[74] M. Berglund, L. Rymell, and H. M. Hertz, "Ultraviolet prepulse for enhanced x-ray emission and brightness from droplet-target laser plasmas," *Applied Physics Letters*, vol. 69, no. 12, pp. 1683–1685, 1996.

[75] M. Anand, S. Kahaly, G. Ravindra Kumar, M. Krishnamurthy, A. S. Sandhu, and P. Gibbon, "Enhanced hard x-ray emission from microdroplet preplasma," *Applied Physics Letters*, vol. 88, no. 18, p. 181111, 2006.

[76] E. A. Ponomareva, A. N. Tcypkin, S. V. Smirnov et al., "Double-pump technique–one step closer towards efficient liquid-based THz sources," *Optics Express*, vol. 27, no. 22, p. 32855, 2019.

[77] E. A. Ponomareva, A. O. Ismagilov, S. E. Putilin, A. N. Tsypkin, S. A. Kozlov, and X. C. Zhang, "Varying pre-plasma properties to boost terahertz wave generation in liquids," *Communications on Physics*, vol. 4, no. 1, article 4, 2021.

[78] H.-H. Huang, T. Nagashima, W.-H. Hsu, S. Juodkazis, and K. Hatanaka, "Dual THz wave and X-ray generation from a water film under femtosecond laser excitation," *Nanomaterials (Basel, Switzerland)*, vol. 8, no. 7, p. 523, 2018.

[79] E. Yiwen, Q. Jin, and X. C. Zhang, "Enhancement of terahertz emission by a preformed plasma in liquid water," *Applied Physics Letters*, vol. 115, no. 10, p. 101101, 2019.

[80] P. M. Solyankin, B. V. Lakatosh, M. S. Krivokorytov et al., "Single free-falling droplet of liquid metal as a source of directional terahertz radiation," *Physical Review Applied*, vol. 14, no. 3, p. 034033, 2020.

[81] J. Kerr, "XL. A new relation between electricity and light: Dielectrified media birefringent," *The London, Edinburgh, and Dublin Philosophical Magazine and Journal of Science*, vol. 50, no. 332, pp. 337–348, 1875.

[82] J. Kerr, "XLIII. On rotation of the plane of polarization by reflection from the pole of a magnet," *The London, Edinburgh, and Dublin Philosophical Magazine and Journal of Science*, vol. 3, no. 19, pp. 321–343, 1877.

[83] M. C. Hoffmann, N. C. Brandt, H. Y. Hwang, K. L. Yeh, and K. A. Nelson, "Terahertz Kerr effect," *Applied Physics Letters*, vol. 95, no. 23, p. 231105, 2009.

[84] F. Perakis, L. de Marco, A. Shalit et al., "Vibrational spectroscopy and dynamics of water," *Chemical Reviews*, vol. 116, no. 13, pp. 7590–7607, 2016.

[85] H. Zhao, Y. Tan, L. Zhang et al., "Ultrafast hydrogen bond dynamics of liquid water revealed by terahertz- induced transient birefringence," *Light: Science & Applications*, vol. 9, no. 1, p. 136, 2020.

[86] R. W. Boyd, *Nonlinear Optics*, Academic press, 2020.

[87] W. Demtröder, *Laser Spectroscopy: vol. 2: Experimental Techniques*, Springer Science & Business Media, 2008.

[88] M. Levenson, *Introduction to Nonlinear Laser Spectroscopy 2e*, Elsevier, 2012.

[89] H. Zhao, Y. Tan, R. Zhang, Y. Zhao, C. Zhang, and L. Zhang, "Anion–water hydrogen bond vibration revealed by the terahertz Kerr effect," *Optics Letters*, vol. 46, no. 2, pp. 230–233, 2021.

[90] I. A. Heisler and S. R. Meech, "Low-frequency modes of aqueous alkali halide solutions: glimpsing the hydrogen bonding vibration," *Science*, vol. 327, no. 5967, pp. 857–860, 2010.

[91] D.-Y. Wu, S. Duan, X.-M. Liu et al., "Theoretical study of binding interactions and vibrational Raman spectra of water in hydrogen-bonded anionic complexes: $(H_2O)_n^-$ (n =2 and 3), $H_2O\cdots X^-$ (X = F, Cl, Br, and I), and $H_2O\cdots M^-$ (M = Cu, Ag, and Au)," *The Journal of Physical Chemistry A*, vol. 112, no. 6, pp. 1313–1321, 2008.

[92] A. V. Grosse, "Surface tension of the alkali metals from the melting point to the critical region," *Journal of Inorganic and Nuclear Chemistry*, vol. 30, no. 5, pp. 1169–1174, 1968.

[93] V. Y. Prokhorenko, V. V. Roshchupkin, M. A. Pokrasin, S. V. Prokhorenko, and V. V. Kotov, "Liquid gallium: potential uses as a heat-transfer agent," *High Temperature*, vol. 38, no. 6, pp. 954–968, 2000.

[94] D. White, "The surface tensions of indium and cadmium," *Metallurgical and Materials Transactions B*, vol. 3, no. 7, pp. 1933–1936, 1972.